European Journal of Chemistry

View Journal Online
View Article Online

Hirshfeld surface and theoretical studies of 2,2,2-trichloro-*N*,*N*-*bis*(2-(2,2,2-trichloroacetamido)phenyl)acetamide compound

Immihan Sezen Aydogdu [1,*], Ilkay Gumus [2] and Hakan Arslan [1]

[1] *Department of Chemistry, Faculty of Arts and Science, Mersin University, Mersin, 33343, Turkey*
immihansezen@gmail.com (I.S.A.), hakan.arslan@mersin.edu.tr (H.A.)
[2] *Department of Basic Sciences, Faculty of Maritime, Mersin University, Mersin, 33343, Turkey*
ilkay.gumus@mersin.edu.tr (I.G.)

* *Corresponding author at: Department of Chemistry, Faculty of Arts and Science, Mersin University, Mersin, 33343, Turkey.*
Tel: +90.505.4574736 Fax: +90.324.3610047 e-mail: immihansezen@gmail.com (I.S. Aydogdu).

RESEARCH ARTICLE

10.5155/eurjchem.10.4.323-335.1920

Received: 24 August 2019
Received in revised form: 17 October 2019
Accepted: 22 October 2019
Published online: 31 December 2019
Printed: 31 December 2019

KEYWORDS

Acetamide
Vibration spectrum
Ab-initio calculations
Redox active compound
Density functional theory
Hirshfeld surface analysis

ABSTRACT

The vibrational frequencies, atomic charges and the related properties of the 2,2,2-trichloro-*N*,*N*-*bis*(2-(2,2,2-trichloroacetamido)phenyl)acetamide (H_2L^{NNN}) were investi-gated by Ab-initio Hartree-Fock (HF) and Density Functional Theory (DFT) methods such as BLYP, B3LYP, B3PW91 and mPW1PW91 functionals with 6-31G(d,p) and 6-311G(d,p) basis sets. The experimentally determined parameters were compared with those calculated theoretically and they were found to complement each other with a very good correlation. The theoretical vibrational spectrum of H_2L^{NNN} molecule was interpreted by means of potential energy distributions using the SQM 2.0 program. The Hirshfeld surface analysis was carried out to discuss the role of the hydrogen bonds and other intermolecular contacts in crystal lattice. Hirshfeld surface analysis revealed the occurrence of Cl···H, Cl···Cl, Cl···C, H···H, O···H, C···H and Cl···π interactions that display an important role on the crystal packing stabilization of the compound.

Cite this: *Eur. J. Chem.* **2019**, *10(4)*, 323-335 **Journal website**: www.eurjchem.com

1. Introduction

The redox active compounds containing amide donors can be modified according to specific needs and most of them have catalytic activity [1-9]. So, in recent years, most of the researchers focused on these types of compounds. Numerous studies have been devoted to investigate how the reactivity of transition metals is affected by a small change in the electron donor property of the ligand [3,4,6]. Redox active compounds have a wide range of uses [2-20]. For complexes of these compounds, a detailed spectroscopic, magnetic, structural and theoretical investigation is used to detect formal oxidation states in metal centers. Recent studies have focused on investigating the importance of the skeleton on unit reactivity rather than understanding the electronic structures of complexes.

In the light of above-mentioned information, our research group focused on the study of redox active compounds. One of them is 2,2,2-trichloro-*N*,*N*-*bis*(2-(2,2,2-trichloroacetamido) phenyl)acetamide (H_2L^{NNN}). The crystal structure of H_2L^{NNN} was obtained using single crystal X-ray diffraction studies [21,22]. Nonetheless, to the best of our knowledge, both Ab-initio studies of the vibrational spectra in the gas phase and the Hirshfeld surface analysis of H_2L^{NNN} have not been reported previously. Thus, we calculated the geometric parameters and vibrational frequencies of H_2L^{NNN} in the ground state to distinguish the fundamentals from the experimental geometric parameters and vibrational frequencies by HF, BLYP, B3LYP, B3PW91 and mPW1PW91 methods with the standard 6-31G(d,p) and 6-311G(d,p) basis sets. A detailed interpretation of the vibrational spectra of H_2L^{NNN} molecule has been made on the basis of the calculated potential energy distribution (PED). We also report detailed analysis of intermolecular interactions by Hirshfeld surfaces analysis. The surfaces are mapped with d_{norm}, 2D-fingerprint plots, shape-index and curvedness properties. The Hirshfeld surface and associated fingerprint plots of H_2L^{NNN} molecule have also provided a platform for the evaluation of the contribution of different atom···atom contacts, which contribute to the packing of the molecules in solids.

2. Experimental

2.1. Instrumentation

ISSN 2153-2249 (Print) / ISSN 2153-2257 (Online) – Copyright © 2019 The Authors – Atlanta Publishing House LLC – Printed in the USA.
This work is published and licensed by Atlanta Publishing House LLC – CC BY NC – Some Rights Reserved.
http://dx.doi.org/10.5155/eurjchem.10.4.323-335.1920

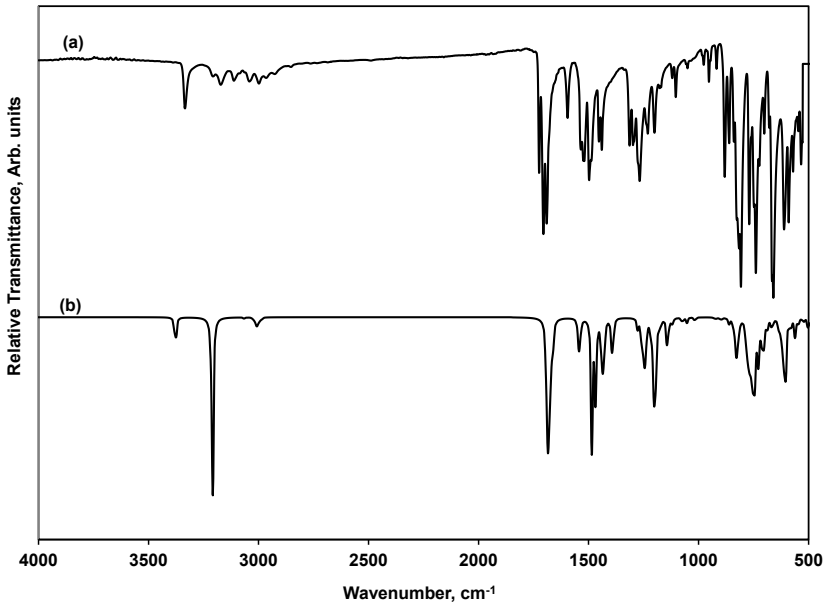

Figure 1. (a) Experimental and (b) theoretical FT-IR spectrum of 2,2,2-trichloro-*N*,*N*-*bis*(2-(2,2,2-trichloroacetamido)phenyl)acetamide compound.

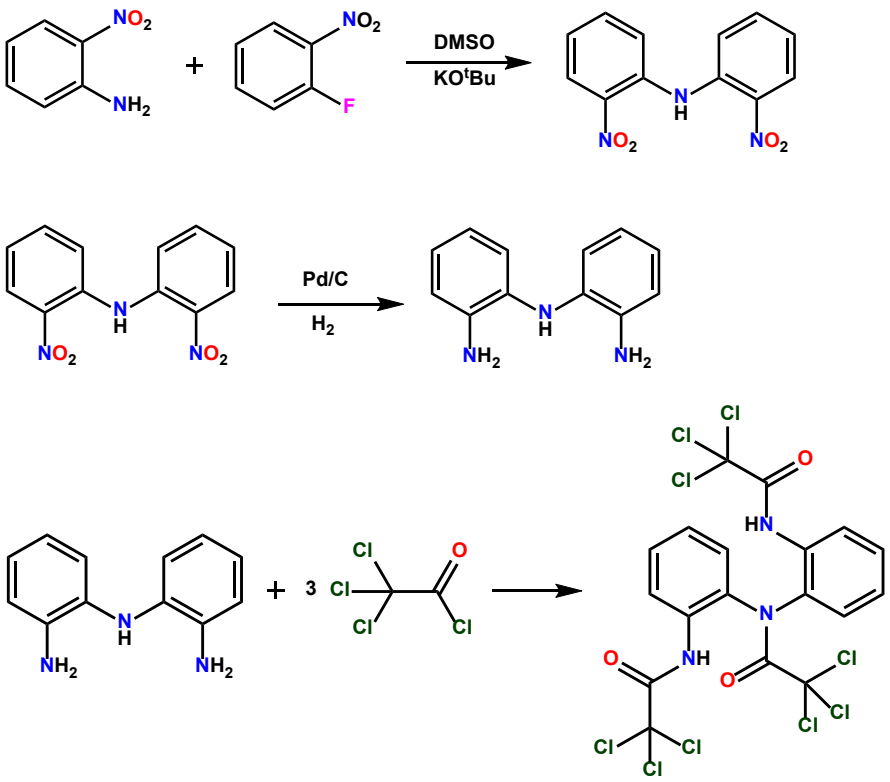

Scheme 1. The synthetic route for 2,2,2-trichloro-*N*,*N*-*bis*(2-(2,2,2-trichloroacetamido)phenyl)acetamide.

The NMR spectra were recorded in Acetone-d_6 solvent on Bruker Avance III 400 MHz NaNoBay FT-NMR spectrophotometer using tetramethylsilane as an internal standard. The room-temperature-attenuated total reflection Fourier transform infrared (FT-IR ATR) spectrum of 2,2,2-trichloro-*N*,*N*-*bis*(2-(2,2,2-trichloroacetamido)phenyl)acetamide compound was recorded using a Perkin Elmer Spectrum 100 series spectrometer with a ATR prism (4000-525 cm^{-1}; number of scans: 200; resolution: 1 cm^{-1}) (Figure 1).

2.2. Synthesis

The solvents and chemicals used in the study were commercially obtained from companies such as Merck, Aldrich and Alfa-Aesar and were used without further purification. Precursor materials *bis*(2-nitrophenyl)amine and *bis*(2-amino phenyl)amine were prepared according to the previously published method (Scheme 1) [21-24]. A solution of trichloro acetyl chloride (10 mmol) in acetonitrile (50 mL) was cooled to 0 °C under nitrogen atmosphere.

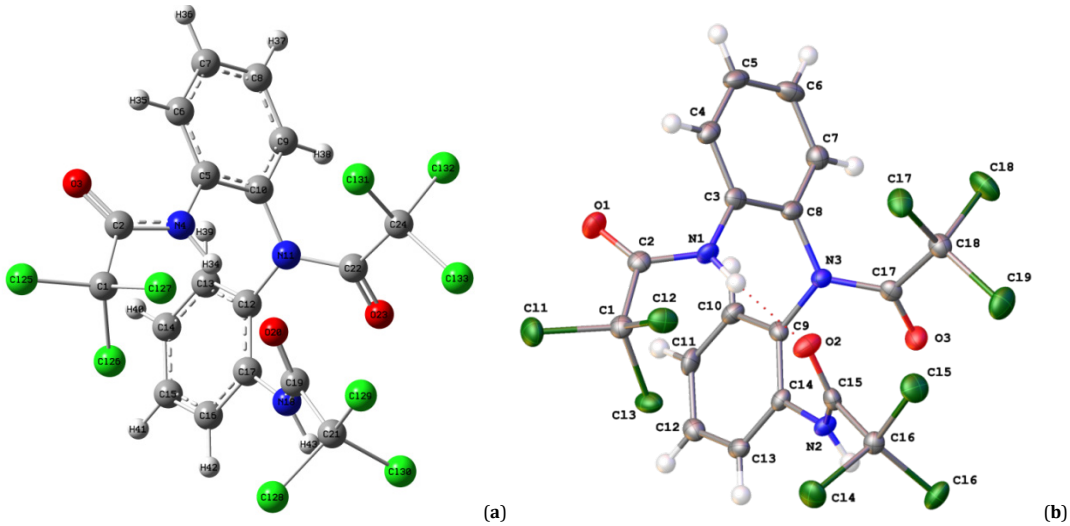

Figure 2. The optimized geometry of H_2L^{NNN} molecule calculated at B3LYP/6-311G (d,p) level (a) and a view of the molecular structure of H_2L^{NNN} molecule with displacement ellipsoids drawn at the 50% probability level (b) [21].

Then, *bis*(2-aminophenyl) amine (5 mmol) was slowly added to this cold solution over 3 hrs. The mixture was stirred at 0 °C for 3 hrs and the mixture temperature was allowed to slowly rise to room temperature. The mixture was stirred at room temperature for 24 hrs and the solvent was removed under vacuum. The final product was crystallized by slow evaporation of the concentrated solution in hot acetone (Scheme 1) [21,22]. 2,2,2-Trichloro-*N*,*N*-*bis*(2-(2,2,2-trichloro acetamido)phenyl) acetamide (H_2L^{NNN}): Color: White. Yield: 43%. ^{1}H NMR (400 MHz, Acetone-d_6, δ, ppm): 10.23 (s, 2H, NH(CO)), 7.82-7.42 (m, 8H, Ar-H).

2.3. Calculation details

The Gaussian 16W program package on a double Xeon/3.2 GHz processor with 16 GB Ram was operated to obtain all calculations [25]. BLYP, B3LYP, B3PW91, mPW1PW91 and HF methods with the standard 6-31G(d,p) and 6-311G(d,p) basis sets were applied to optimize the molecular structure of 2,2,2-trichloro-*N*, *N*-*bis*(2-(2, 2, 2-trichloroacetamido)phenyl) acetamide molecule in the ground state. These methods were also used to calculate the vibrational frequencies. The frequency values computed at these levels contain known systematic errors [26]. Scaling factor values of 0.9614, 0.9679, 0.9573, 0.9631, 0.9945, 0.9934, 0.8992, 0.9051, 0.9500 and 0.9567 for B3LYP/6-31G(d,p), B3LYP/6-311G(d,p), B3PW91/6-31G(d,p), B3PW91/6-311G(d,p), BLYP/6-31G(d,p), BLYP/6-311G(d,p), HF/6-31G(d,p), HF/6-311G(d,p), mPW1PW91/6-31G(d,p) and mPW1PW91/6-311G(d,p), respectively, can be used to correct these discrepancies [27-33]. Also, optimal scaling factors were calculated for all analyzed methods. The GaussView 6.0 graphical interface of the Gaussian program, which is an animation option that provides a visual representation of the shape of the modes of vibration, provides a way of assigning the calculated wavenumbers [34]. The SQM procedure has been widely used in the assignment of bands of vibrational spectra due to being a highly successful and well established technique in refining the computerized vibration frequencies to match the experimental values better [35]. So, the vibrational modes were determined according to the potential energy distribution analysis using the SQM program [36]. Using the PAVF 1.0 program, the performance of the used method was quantitatively characterized [37]. The population analysis has also been performed by the natural bond orbital method [38] at B3LYP, BLYP, B3PW91, mPW1PW91 and HF /6-31G(d,p) and 6-311G(d,p) level of theory using the natural bond orbital (NBO) program [39] under the Gaussian 16W program package.

2.4. Hirshfeld surfaces analysis

Analysis of Hirshfeld surfaces and their associated two dimensional fingerprint plots of 2,2,2-trichloro-*N*,*N*-*bis*(2-(2,2,2-trichloroacetamido)phenyl)acetamide molecule were calculated by using the CrystalExplorer 17 [40]. The Hirshfeld surfaces are mapped with different properties d_{norm}, shape index and curvedness. The d_{norm} is normalized contact distance, defined in terms of d_e, d_i and the vdW radii of the atoms. The combination of d_e and d_i in the form of a 2D fingerprint plot displays the summary of intermolecular contacts in the crystal.

3. Results and discussion

3.1. Molecular geometry

The title compound was prepared according to the previously published method (Scheme 1) [21]. It was characterized by Nuclear Magnetic Resonance spectroscopy (NMR) and Fourier Transform Infrared Spectroscopy (FTIR) techniques. All the obtained characterization data agree with both the literature data [21] and the structure proposed for the title compound. The molecular structure of the 2,2,2-trichloro-*N*, *N*-*bis*(2-(2, 2, 2-trichloroacetamido)phenyl)acetamide obtained by the single crystal X-ray diffraction method has been previously reported [21,22]. The compound crystallizes monoclinic, space group $P2_1/n$, a = 12.3377(6) Å, b = 12.3897(5) Å, c = 15.4444(7) Å, β = 93.849(2)°, V = 2355.51(18) Å^3, Z = 4 and D_{calc} = 1.792 g/cm^3. The molecular structure of H_2L^{NNN} compound belongs to C_1 point group symmetry.

Figure 2 demonstrates the single crystal structure and the optimized molecular structure of H_2L^{NNN} molecule which was obtained from the GaussView 6.0 program [34]. Table 1 lists the optimized structure parameters of H_2L^{NNN} compound calculated by B3LYP, BLYP, B3PW91, mPW1PW91 and HF methods with the standard 6-31G(d,p) and 6-311G(d,p) basis sets. At the optimized geometry for H_2L^{NNN} molecule, no imaginary frequency modes were obtained, therefore a true minimum on the potential energy surface was found.

Table 1. Optimized and experimental geometries of H_2L^{NNN} molecule in the ground state *.

Parameter	Experimental, Å	Calculated, Å									
		B3LYP		B3PW91		BLYP		HF		mPW1PW	
		6-31	6-311	6-31	6-311	6-31	6-311	6-31	6-311	6-31	6-311
Bond lengths											
C1-C2	1.569(2)	1.580	1.580	1.575	1.573	1.595	1.597	1.564	1.563	1.571	1.569
C1-Cl25	1.761(2)	1.781	1.780	1.769	1.766	1.803	1.802	1.762	1.762	1.764	1.761
C1-Cl26	1.774(2)	1.810	1.809	1.795	1.794	1.841	1.838	1.776	1.777	1.789	1.788
C1-Cl27	1.774(2)	1.800	1.798	1.786	1.784	1.827	1.825	1.771	1.772	1.781	1.779
C2-O3	1.206(2)	1.214	1.206	1.212	1.205	1.227	1.219	1.188	1.181	1.209	1.202
C2-N4	1.356(2)	1.367	1.367	1.363	1.363	1.380	1.380	1.355	1.356	1.360	1.360
N4-C5	1.414(2)	1.412	1.412	1.406	1.405	1.423	1.423	1.412	1.412	1.403	1.402
C5-C6	1.396(2)	1.403	1.401	1.401	1.398	1.415	1.412	1.389	1.388	1.399	1.396
C5-C10	1.403(2)	1.414	1.411	1.411	1.409	1.427	1.424	1.398	1.397	1.409	1.406
C6-C7	1.392(3)	1.393	1.391	1.391	1.389	1.402	1.399	1.383	1.383	1.389	1.387
C7-C8	1.383(3)	1.393	1.390	1.391	1.388	1.403	1.400	1.381	1.380	1.389	1.386
C8-C9	1.388(2)	1.392	1.389	1.390	1.387	1.402	1.399	1.382	1.381	1.388	1.386
C9-C10	1.389(2)	1.397	1.394	1.395	1.392	1.408	1.405	1.387	1.385	1.392	1.389
C10-N11	1.442(2)	1.445	1.444	1.438	1.436	1.457	1.456	1.439	1.439	1.435	1.433
N11-C12	1.443(2)	1.445	1.444	1.438	1.435	1.458	1.457	1.437	1.437	1.435	1.433
N11-C22	1.376(2)	1.390	1.391	1.386	1.386	1.406	1.407	1.384	1.385	1.382	1.382
C12-C13	1.398(2)	1.402	1.399	1.400	1.397	1.413	1.409	1.387	1.386	1.399	1.395
C12-C17	1.403(2)	1.413	1.408	1.410	1.406	1.425	1.420	1.395	1.394	1.408	1.404
C13-C14	1.380(2)	1.390	1.388	1.388	1.386	1.400	1.398	1.383	1.383	1.386	1.384
C14-C15	1.389(2)	1.393	1.391	1.392	1.389	1.404	1.401	1.381	1.380	1.390	1.387
C15-C16	1.385(2)	1.389	1.387	1.387	1.385	1.399	1.397	1.382	1.382	1.385	1.383
C16-C17	1.395(2)	1.401	1.397	1.400	1.395	1.413	1.408	1.385	1.384	1.398	1.394
C17-N18	1.432(2)	1.425	1.427	1.418	1.419	1.434	1.436	1.428	1.428	1.415	1.416
N18-C19	1.341(2)	1.349	1.349	1.346	1.345	1.363	1.362	1.339	1.340	1.343	1.343
C19-O20	1.219(2)	1.219	1.211	1.217	1.210	1.232	1.224	1.191	1.185	1.214	1.208
C19-C21	1.561(2)	1.575	1.574	1.571	1.568	1.590	1.591	1.563	1.561	1.567	1.564
C21-Cl28	1.780(2)	1.811	1.808	1.797	1.794	1.838	1.836	1.778	1.780	1.791	1.789
C21-Cl29	1.766(2)	1.772	1.771	1.760	1.758	1.791	1.790	1.756	1.756	1.755	1.754
C21-Cl30	1.766(2)	1.808	1.807	1.794	1.792	1.841	1.839	1.777	1.777	1.788	1.786
C22-O23	1.207(2)	1.212	1.205	1.211	1.204	1.225	1.218	1.184	1.177	1.208	1.201
C22-C24	1.574(2)	1.585	1.586	1.580	1.579	1.599	1.601	1.575	1.575	1.576	1.575
C24-Cl31	1.766(2)	1.790	1.788	1.776	1.774	1.816	1.814	1.765	1.765	1.771	1.769
C24-Cl32	1.777(2)	1.812	1.808	1.798	1.794	1.842	1.838	1.776	1.776	1.792	1.788
C24-Cl33	1.779(2)	1.797	1.798	1.784	1.784	1.821	1.822	1.775	1.776	1.778	1.778
r		0.9993	0.9994	0.9993	0.9993	0.9986	0.9989	0.9994	0.9992	0.9993	0.9994
Bond angles											
C2-C1-Cl25	109.98(12)	109.56	109.50	109.35	109.37	109.61	109.51	109.70	109.77	109.33	109.37
C2-C1-Cl26	109.89(12)	109.46	109.48	109.47	109.41	109.71	109.75	108.41	108.43	109.42	109.32
C2-C1-Cl27	109.34(12)	109.68	109.81	109.43	109.51	109.81	110.02	110.72	110.59	109.35	109.44
Cl25-C1-Cl26	108.50(9)	108.74	108.72	108.92	108.93	108.53	108.50	108.82	108.81	108.99	109.00
Cl25-C1-Cl27	109.29(9)	109.29	109.27	109.45	109.49	109.19	109.14	108.76	108.88	109.52	109.56
Cl26-C1-Cl27	109.82(9)	110.09	110.04	110.21	110.13	109.97	109.89	110.42	110.34	110.20	110.13
C1-C2-O3	120.24(15)	119.23	119.30	119.27	119.47	119.16	119.18	118.99	119.18	119.34	119.55
C1-C2-N4	113.42(14)	114.64	114.54	114.56	114.33	114.65	114.61	115.55	115.22	114.43	114.20
O3-C2-N4	126.34(16)	126.13	126.16	126.18	126.20	126.20	126.21	125.45	125.60	126.23	126.25
C2-N4-C5	123.21(14)	124.39	124.19	124.28	124.14	124.59	124.33	122.50	122.78	124.35	124.20
N4-C5-C6	120.99(16)	122.21	122.03	122.40	122.27	122.09	121.86	120.86	121.02	122.59	122.47
N4-C5-C10	120.16(15)	119.52	119.81	119.39	119.58	119.72	120.09	120.77	120.63	119.12	119.32
C6-C5-C10	118.84(16)	118.26	118.15	118.20	118.14	118.17	118.04	118.36	118.34	118.27	118.21
C5-C6-C7	120.39(15)	120.78	120.91	120.78	120.85	120.87	121.01	121.08	121.08	120.65	120.74
C6-C7-C8	120.42(16)	120.80	120.74	120.86	120.80	120.79	120.72	120.45	120.46	120.92	120.86
C7-C8-C9	119.63(17)	118.97	118.94	118.92	118.92	119.01	118.96	118.92	118.87	118.94	118.93
C8-C9-C10	120.54(17)	120.98	121.06	120.95	120.98	121.04	121.14	121.21	121.25	120.85	120.88
C5-C10-C9	120.07(16)	120.15	120.15	120.25	120.26	120.08	120.06	119.88	119.92	120.33	120.33
C5-C10-N11	120.39(15)	121.02	121.28	120.87	121.04	121.23	121.54	121.57	121.54	120.61	120.80
C9-C10-N11	119.46(16)	118.71	118.45	118.74	118.57	118.56	118.27	118.52	118.51	118.91	118.73
C10-N11-C12	117.13(13)	116.40	116.61	116.30	116.53	116.35	116.56	117.05	117.11	116.27	116.49
C10-N11-C22	123.75(14)	123.28	122.39	123.12	122.42	123.27	122.44	119.91	119.51	123.34	122.65
C12-N11-C22	115.88(14)	116.61	116.55	116.73	116.77	116.39	116.33	115.73	115.75	116.96	116.98
N11-C12-C13	118.00(16)	118.18	118.73	118.14	118.59	118.19	118.67	119.95	120.06	117.99	118.43
N11-C12-C17	123.01(15)	123.71	122.96	123.72	123.08	123.71	123.08	121.41	121.33	123.90	123.28
C13-C12-C17	118.99(16)	118.11	118.30	118.13	118.33	118.09	118.25	118.61	118.59	118.09	118.29
C12-C13-C14	121.22(16)	121.91	121.64	121.92	121.66	121.91	121.68	121.17	121.21	121.96	121.71
C13-C14-C15	119.79(16)	119.82	119.90	119.80	119.86	119.83	119.90	120.13	120.09	119.79	119.85
C14-C15-C16	119.71(16)	119.10	119.16	119.09	119.16	119.15	119.21	119.10	119.09	119.06	119.13
C15-C16-C17	121.11(16)	121.73	121.50	121.75	121.55	121.70	121.51	121.20	121.22	121.80	121.60
C12-C17-C16	119.14(15)	119.30	119.46	119.28	119.39	119.27	119.41	119.78	119.80	119.26	119.36
C12-C17-N18	125.11(15)	125.76	124.82	125.67	124.85	125.80	124.99	123.67	123.54	125.83	125.03
C16-C17-N18	115.72(16)	114.86	115.66	115.00	115.72	114.87	115.56	116.46	116.60	114.86	115.57
C17-N18-C19	125.61(14)	127.95	126.83	127.71	126.80	128.24	127.27	124.79	124.60	127.75	126.86
N18-C19-O20	126.42(16)	126.33	126.25	126.39	126.34	126.49	126.48	125.62	125.58	126.36	126.30
N18-C19-C21	116.26(14)	114.17	114.35	113.97	114.12	114.02	114.09	115.80	115.63	113.95	114.09
O20-C19-C21	117.24(15)	119.41	119.29	119.53	119.42	119.40	119.33	118.44	118.67	119.60	119.49
C19-C21-Cl28	105.86(11)	106.40	106.09	106.34	105.92	106.43	106.26	105.40	105.34	106.40	105.96
C19-C21-Cl29	109.60(12)	110.26	110.17	110.09	110.05	110.42	110.34	110.14	110.11	110.05	110.02
C19-C21-Cl30	113.19(12)	111.82	112.24	111.71	112.05	112.10	112.46	113.34	113.32	111.49	111.84
Cl28-C21-Cl29	108.61(9)	109.90	109.85	109.99	109.94	109.91	109.81	109.99	109.95	109.98	109.94

Table 1. Continued.

Parameter	Experimental, Å	Calculated, Å									
		B3LYP		B3PW91		BLYP		HF		mPW1PW	
		6-31	6-311	6-31	6-311	6-31	6-311	6-31	6-311	6-31	6-311
Cl28-C21-Cl30	110.44(9)	108.86	108.91	108.93	109.07	108.54	108.58	108.81	108.86	109.04	109.17
Cl29-C21-Cl30	109.01(9)	109.54	109.50	109.72	109.74	109.38	109.31	109.09	109.17	109.81	109.83
N11-C22-O23	122.91(16)	122.50	122.88	122.56	122.88	122.50	122.88	123.28	123.43	122.54	122.84
N11-C22-C24	119.77(14)	120.83	120.25	120.61	120.04	120.74	120.27	120.37	119.91	120.56	120.02
O23-C22-C24	117.14(15)	116.61	116.77	116.78	117.00	116.69	116.75	116.24	116.54	116.86	117.06
C22-C24-Cl31	115.16(12)	116.31	116.46	116.10	116.28	116.76	117.04	115.77	115.85	115.93	116.12
C22-C24-Cl32	109.41(12)	107.62	107.81	107.60	107.69	107.55	107.68	108.47	108.46	107.57	107.66
C22-C24-Cl33	106.30(12)	107.19	106.80	107.01	106.65	107.28	106.88	106.74	106.62	107.04	106.71
Cl31-C24-Cl32	110.36(10)	109.85	109.82	109.99	109.98	109.66	109.57	109.87	109.86	110.04	110.04
Cl31-C24-Cl33	107.66(9)	107.56	107.59	107.78	107.83	107.43	107.43	107.45	107.54	107.85	107.89
Cl32-C24-Cl33	107.59(9)	108.02	108.05	108.08	108.10	107.83	107.89	108.27	108.24	108.13	108.13
r		0.9886	0.9908	0.9885	0.9906	0.9877	0.9891	0.9851	0.9846	0.9880	0.9904

* 6-31: 6-31G(d,p); 6-311: 6-311G(d,p); The atom numbering scheme given in Figure 2(a).

As a result, the unscaled calculated frequencies, reduced masses, force constants and infrared intensities are obtained. It can be said that X-ray single crystal geometrical parameters fairly well reproduced the optimized geometry when the theoretical and experimental geometry of H_2L^{NNN} compound was compared to each other. Based on this comparison, the bond lengths and angles calculated for H_2L^{NNN} compound show good agreement with experiment one. According to our calculations, the optimized bond lengths and bond angles obtained by mPW1PW91/6-311G(d,p) and B3LYP/6-311G (d,p) methods, respectively, show the best agreement with the experimental values. The largest difference between experimental and calculated bond lengths and bond angles are 0.020 Å and 2.05 °, respectively [21].

3.2. Vibrational assignments

The vibrational frequencies obtained by HF and DFT calculation methods are summarized in Table 2 along with the approximate description of each of the normal modes and experimental frequencies (Figure 1). Usually, anharmonicity of the incomplete incorporation of electron correlation and of the use of finite one-particle basis set causes the calculated harmonic vibrational wavenumbers to be higher than the experimental values [27]. For this reason, the scaling factors of 0.9614, 0.9679, 0.9573, 0.9631, 0.9945, 0.9934, 0.8992, 0.9051, 0.9500 and 0.9567 were used for B3LYP/6-31G(d,p), B3LYP/6-311G(d,p), B3PW91/6-31G(d,p), B3PW91/6-311G (d,p), BLYP/6-31G(d,p), BLYP/6-311G(d,p), HF/6-31G(d,p), HF/6-311G(d,p), mPW1PW91/6-31G(d,p) and mPW1PW91/ 6-311G(d,p) levels, respectively [27-33]. The vibrational bands' assignments have been made by using both the animation option of the GaussView 6.0 graphical interface for the Gaussian programs [34] and SQM 2.0 program [36]. All the calculated spectra were found to be in good accordance with the experimental ones. Considering Table 2, it can be concluded that experimental bases better aligned with the scaled fundamentals and have a better correlation with B3LYP/6-31G(d,p) than the other calculations methods.

A general and better performance of the used calculation methods can be quantitatively characterized by using the mean absolute percentage error, mean absolute error, root mean square values (RMS) and coefficients of correlation (*r*) between the theoretically calculated and experimentally observed vibration frequencies (Table 3). All these values were calculated in this study by the PAVF 1.0 program [37] according to Scott and Radom [27]. The RMS values were obtained in this study using Equation (1) [27,41]. The *r* values for all DFT methods were greater than 0.9987. These values are very close to those reported in literature [28,42,43]. The RMS error of the observed and calculated IR bands is given in Table 3. These results indicate that the fundamental frequencies calculated by the selected methods (except HF) and basis sets for H_2L^{NNN} compound show good agreement with experimental values. Especially, the B3LYP method with 6-31G(d,p) basis set has the best agreement. We observed a small difference between experimental and theoretical vibrational modes. This discrepancy is due to the formation of the intermolecular and intramolecular hydrogen bonding. Also, we note that the experimental results belong to the solid phase and the theoretical results belong to the gaseous phase. Finally, we calculated the optimal scaling factors, which are crucial for IR spectral predictions, using the PAVF 1.0 program [37]. Without accounting for different vibrations, only single-uniform scaling factors were calculated. The values obtained are 0.9588, 0.9639, 0.9545, 0.9594, 0.9924, 0.9973, 0.8928, 0.8981, 0.9473 and 0.9522 for the B3LYP/6-31G(d,p), B3LYP/6-311G(d,p), B3PW91/6-31G(d,p), B3PW91/6-311G(d,p), B-LYP/6-31G(d,p), B-LYP/6-311G(d,p), HF/6-31G(d,p), HF/6-311G(d,p), mPW1PW91/6-31G(d,p) and mPW1PW91/ 6-311G (d,p) methods, respectively. They are very close to those recommended by Scott and Radom [27] for the same level of theory.

$$RMS = \sqrt{\frac{1}{n-1}\sum_{i}^{n}\left(\nu_i^{calc} - \nu_i^{exp}\right)^2} \quad (1)$$

The ν_{NH} stretching vibration bands are generally observed in the 3500-3000 cm^{-1} region of the FT-IR spectrum for heterocyclic compounds [23,44,45]. In this study, the stretching vibration mode of ν_{NH} groups of H_2L^{NNN} molecule in FT-IR spectrum were observed at 3335 and 3291 cm^{-1}. ν_{NH} stretching vibration modes were calculated by B3LYP/6-31G(d,p) method as 3469 and 3296 cm^{-1} (Table 2). The differences between the experimentally observed and theoretically calculated ν_{NH} stretching vibration bands were found to be 134 and 5 cm^{-1}, respectively, and these differences were related to the hydrogen bond N-H···O=C occurring between the molecules [23,44,45]. The hydrogen bond (N-H···O=C) between the molecules of H_2L^{NNN} was also confirmed by the deviation in the νC=O stretching vibration mode. The $\nu_{C=O}$ stretching vibration modes were observed at 1728, 1725 and 1706 cm^{-1}, whereas theoretically related $\nu_{C=O}$ stretching vibration modes were calculated at 1737, 1727 and 1710 cm^{-1}, respectively. The differences between the calculated and observed stretching modes are 9, 2 and 4 cm^{-1}, respectively (Table 2). These results are confirmed by the presence of intermolecular hydrogen bonds in the single crystal structure of the compound [21].

The characteristic ν_{CH} stretching vibrations of aromatic structure are expected to appear in 3000-3100 cm^{-1} frequency ranges. The ν_{CH} stretching vibrations of the title compound were assigned to seven bands observed at 3155, 3112, 3101, 3095, 3082, 3078, and 3064 cm^{-1} in the infrared spectrum. The B3LYP/6-31G(d,p) calculated theoretical wave-numbers of these bands reproduced the experimental ones very well.

Table 2. Vibrational wavenumbers obtained for H_2L^{NNN} at 6-31G(d,p) level.

No	Exp. IR (cm^{-1})	B3LYP				Assignments, PED (%)
		Unscaled (cm^{-1})	Scaled (cm^{-1})	Scaled (cm^{-1})	IR Int. (km/mol)	
1	3335	3608	3469	3460	70.00	νNH_{18}, 100
2	3291	3428	3296	3287	424.28	νNH_4, 99
3	3155	3275	3149	3140	2.26	νCH_{arom}, 99, sym
4	3112	3233	3108	3100	2.46	νCH_{arom}, 90, sym
5	3101	3224	3099	3091	3.30	νCH_{arom}, 96, sym
6	3095	3217	3093	3084	11.33	νCH_{arom}, 86, asym
7	3082	3210	3086	3078	16.69	νCH_{arom}, 99, asym
8	3078	3202	3078	3070	4.54	νCH_{arom}, 96, asym
9	3078	3195	3072	3064	2.72	νCH_{arom}, 96, asym
10	3064	3189	3066	3057	2.83	νCH_{arom}, 95, asym
11	1728	1806	1737	1732	109.6	νCO_3, 76
12	1725	1796	1727	1722	418.59	νCO_{19}, 65
13	1706	1778	1710	1705	109.42	νCO_{22}, 81
14	1596	1657	1593	1589	7.90	νCC_{arom}, 58
15	1589	1654	1590	1586	1.69	νCC_{arom}, 53
16	1586	1646	1583	1579	85.73	νCC_{arom}, 38 + δCNH, 12 + δCCC, 11
17	1582	1638	1574	1570	4.65	νCC_{arom}, 41 + δCNH, 12
18	1524	1586	1525	1521	278.07	νCC_{arom}, 12 + δCNH, 44
19	1498	1568	1507	1503	173.34	νNC_{arom}, 16 + δCNH, 54
20	1487	1537	1477	1473	154.21	νNC_{arom}, 21 + δCH_{arom}, ipb, 52 + δCCC, 21
21	1452	1524	1465	1462	47.67	δCNH, 22 + δCCH, 45
22	1440	1490	1432	1428	66.52	δCH_{arom}, ipb, 43 + νCC_{arom}, 24
23	1428	1480	1423	1419	27.35	δCH_{arom}, ipb, 48 + νCC_{arom}, 22
24	1313	1363	1310	1307	23.77	νCC_{arom}, 63
25	1293	1342	1290	1286	93.02	νCC_{arom}, 69
26	1278	1330	1278	1275	79.08	νCC_{arom}, 21 + νCN, 14 + δCH_{arom}, ipb, 41
27	1268	1323	1272	1268	37.52	νCC_{arom}, 20 + νCN, 10 + δCH_{arom}, ipb, 45
28	1253	1297	1247	1243	55.48	νCN, 38 + δCH_{arom}, ipb, 21
29	1231	1283	1233	1230	183.56	νCC_{arom}, 19 + νCN, 24 + δCNH, 20
30	1224	1275	1226	1222	92.55	νCN, 35 + δCNH, 11 + δCH_{arom}, ipb, 28
31	1200	1254	1206	1203	20.01	νCN, 27 + δCH_{arom}, ipb, 33
32	1176	1220	1173	1169	57.81	νCN, 35 + δCH_{arom}, ipb, 42
33	1169	1218	1171	1168	19.64	νCN, 28 + δCH_{arom}, ipb, 45 + νCC_{Cl}, 11
34	1156	1199	1153	1150	11.33	νCC_{arom}, 24 + δCH_{arom}, ipb, 45 + νCC_{Cl}, 14
35	1145	1196	1150	1146	0.79	νCC_{arom}, 14 + δCH_{arom}, ipb, 46
36	1145	1192	1146	1143	5.41	νCC_{arom}, 10 + δCH_{arom}, ipb, 48 + νCC_{Cl}, 13
37	1103	1147	1103	1100	12.18	νCC_{arom}, 11 + δCH_{arom}, ipb, 42
38	1087	1125	1081	1078	11.24	νCC_{arom}, 11 + δCH_{arom}, ipb, 42
39	1049	1087	1045	1042	4.15	νCC_{arom}, 45 + νCC_{Cl}, 10
40	1038	1084	1042	1039	3.98	νCC_{arom}, 42
41	952	997	958	956	0.27	δCH_{arom}, opb, 75
42	952	993	954	952	0.20	δCH_{arom}, opb, 79
43	945	986	948	945	3.82	δCH_{arom}, opb, 35 + δCCC, 21 + νCC, 20 + νCC_{Cl}, 12
44	942	977	939	936	0.50	νCC_{Cl}, 32 + δOCN, 23 + νCC, 35
45	921	963	926	923	2.13	δCH_{arom}, opb, 24 + νCC_{Cl}, 19
46	918	958	921	918	0.84	δCH_{arom}, opb, 35 + νCC_{Cl}, 12 + δCNH, 28
47	918	956	919	916	2.05	δCH_{arom}, opb, 46 + νCC_{Cl}, 13
48	882	921	885	883	11.51	δCCC_{ring}, 65 + νCN, 21 + δCH_{arom}, opb, 12
49	860	897	862	860	22.27	δCH_{arom}, opb, 46 + νCC, 11 + δCCN, 20
50	856	887	852	850	67.09	δCH_{arom}, opb, 22 + δCCC_{ring}, 35 + νCC_{Cl}, 11
51	842	881	847	844	34.39	δCH_{arom}, opb, 51 + δCCN, 22
52	840	873	839	837	31.59	δCH_{arom}, opb, 58 + δCCN, 24
53	808	834	802	800	90.63	νCCl, 61 + δCCN, 17 + δNH, opb, 16
54	798	823	791	789	76.55	νCCl, 52 + δNH, opb, 40
55	786	814	782	780	67.37	νCCl, 50 + δCH_{arom}, opb, 22 + δCCC_{ring}, 12
56	773	807	776	773	63.70	νCCl, 44 + δCH_{arom}, opb, 20 + δCCC_{ring}, 15
57	770	805	773	771	52.04	γC-C_{Carb}, 39 + νCCl, 16
58	759	796	766	764	127.74	γC-C_{Carb}, 38 + νCCl, 17
59	752	783	753	751	27.65	δCH_{arom}, opb, 71
60	749	780	750	748	63.3	δCH_{arom}, opb, 64
61	740	774	744	742	41.66	δCH_{arom}, opb, 62 + γC-C_{Carb}, 12
62	735	761	732	730	42.12	δCH_{arom}, opb, 60 + γNH, 17 + δCCC_{ring}, 10
63	723	752	723	721	52.11	δCH_{arom}, opb, 44 + γC-C_{Carb}, 42
64	716	742	713	711	4.30	γNH, 58 + δCH_{arom}, opb, 13
65	702	735	706	705	18.97	γNH, 69 + δCH_{arom}, opb, 23
66	679	712	684	682	25.34	γNH, 47 + δCH_{arom}, opb, 21 + νCCl, 15
67	660	675	649	647	39.47	δCCC_{ring}, 38 + δCH_{arom}, opb, 21 + δNCO, 11
68	636	659	634	632	65.29	δCCC_{ring}, 20 + γC, 45 + νCCl, 19
69	621	651	626	624	62.23	δCCC_{ring}, 10 + γC, 25 + νCCl, 46
70	612	646	621	620	119.36	δCCC_{ring}, 11 + γC, 27 + νCCl, 40
71	591	622	598	596	26.63	δCCC_{ring}, 39 + γC, 21
72	571	599	576	574	41.29	δCCC_{ring}, 44 + γC, 22
73	559	583	560	559	9.81	δCCC_{ring}, 47 + γC, 26
74	-	559	538	536	6.49	γC, 26 + γNH, 37 + δCCC_{ring}, 22
75	-	556	535	533	3.04	γC, 33 + γNH, 31 + δCCC_{ring}, 20
76	-	535	515	513	25.16	γC, 30 + γNH, 19
77	-	521	501	499	13.95	γC, 21 + γNH, 27
78	-	501	481	480	3.35	γC, 29 + τCC_{ring}, 43

Table 2. Continued.

No	Exp. IR (cm^{-1})	B3LYP				Assignments, PED (%)
		Unscaled (cm^{-1})	Scaled (cm^{-1})	Scaled (cm^{-1})	IR Int. (km/mol)	
79	-	484	465	464	7.61	τCC_{ring}, 48 + γNH, 12
80	-	470	452	450	6.14	δCCN, 40 + γC, 36
81	-	444	427	426	5.72	γNH, 25 + δCCN, 30
82	-	429	412	411	0.85	νCCl_{sym}, 54 + δCNC, 32
83	-	422	406	405	6.22	δCCO, 28 + νCCl_{sym}, 21 + δCCN, 12
84	-	416	400	399	3.59	δNCO, 23 + νCCl_{sym}, 27 + δCCN, 20
85	-	377	362	361	0.95	δClCCl, 35 + δCCC_{ring}, 20 + νCCl, 17
86	-	369	355	354	2.15	δClCCl, 40 + δCCC_{ring}, 22 + νCCl, 26
87	-	359	345	344	1.01	δClCCl, 40 + δCCC_{ring}, 22
88	-	345	331	331	0.25	γC_{ring}, 41 + τCC, 40
89	-	336	323	322	3.45	δCCC_{ring}, 14 + τCC, 12 + δOCC, 21
90	-	315	302	302	3.46	γC_{ring}, 26 + γCN, 25 + τCC, 20
91	-	304	293	292	2.18	τCC, 22 + γCN, 20 + γC, 15 + $\delta ClCCl_{scis}$, 32
92	-	295	284	283	1.73	$\delta CCCl_{scis}$, 36 + δNCO, 19
93	-	288	277	276	0.79	$\delta ClCCl_{scis}$, 31 + τCC, 29
94	-	283	272	272	0.99	τCC, 22 + δClCCl, 38
95	-	280	269	269	0.58	γC, 26 + $\delta ClCCl_{scis}$, 39
96	-	267	256	256	0.57	γNH, 31 + $\delta CCCl_{scis}$, 40 τCC, 18
97	-	259	249	248	3.13	γNH, 27 + $\delta CCCl_{scis}$, 42
98	-	239	230	229	1.18	$\delta CCCl_{scis}$, 44 + τNC, 22 + γC, 28
99	-	230	221	220	0.35	δCCCl, 33 + τNC, 16 + γC, 22
100	-	221	213	212	0.23	δCCCl, 40 + τNC, 16
101	-	203	195	194	0.20	$\delta CCCl_{twist}$, 29 + τNC, 18
102	-	197	190	189	2.35	τCC, 32
103	-	187	180	180	7.45	τCC_{Cl}, 32
104	-	167	161	160	1.52	δNCC_{ring}, 41 + τNC, 19 + $\delta CCCl_{twist}$, 20
105	-	166	159	159	0.47	τNC, 18 + τCC_{Cl}, 10 + δCNC, 12 + $\delta CCCl_{twist}$, 12
106	-	157	151	150	2.73	τNC_{ring}, 15 + τCC_{Cl}, 15 + δCNC, 14
107	-	142	137	136	1.34	τNC_{ring}, 26 + τCC_{Cl}, 11 + δCNC, 10
108	-	141	136	136	2.38	τNC_{ring}, 26 + τCN, 15 + δCNC, 13
109	-	130	125	125	4.47	τNC_{ring}, 47 + τCN, 13 + $\delta CCCl_{wagg}$, 12
110	-	100	96	96	0.92	τNC_{ring}, 24 + τCN, 32
111	-	96	92	92	1.36	τCN, 30 + δCNC, 15 + $\delta CCCl_{wagg}$, 12
112	-	91	88	88	0.81	τCN, 28 + δCNC, 12
113	-	80	77	77	1.23	τCN, 44 + τCC, 10 + τCC_{Cl}, 11 + δCNC, 15
114	-	69	67	66	0.23	τCC, 35 + δCNC, 15
115	-	47	46	45	0.28	τCN, 44 + τCC, 10 + τCC_{Cl}, 11
116	-	47	45	45	0.43	τCN, 11 + τCC, 40
117	-	45	43	43	0.45	τCN, 51
118	-	42	40	40	0.27	τNC_{ring}, 56 + $\delta CCCl_{rock}$, 12
119	-	35	33	33	0.49	τCN, 28 + τCC, 38
120	-	31	30	30	0.35	τCC, 39 + τNC_{ring}, 37 + $\delta CCCl_{rock}$, 13
121	-	28	27	27	0.45	τCN, 40 + τCC, 25 + $\delta CCCl_{rock}$, 15
122	-	19	18	18	0.03	τCN, 41 + τCC, 37 + $\delta CCCl_{rock}$, 16
123	-	15	14	14	0.38	τCN, 43
r		0.9998	0.9998	0.9998		
Mean absolute percentage error		4.1492	0.4407	0.4648		
Mean absolute error		55.9474	5.8136	6.6174		
RMS		52.4182	12.5792	12.1672		
Scaling factor		1.000	0.9614	0.9588		

* ν, stretching; δ, in-plane bending; γ, out-of-plane bending; τ, torsion; ipb: in-plane bending; opb: out-of-plane bending; scis: scissoring; wagg: wagging; twist: twisting; rock: rocking; sym, symmetric; asym, asymmetric; arom: aromatic; carb: carbonyl group; PED less than 10% are not shown.

The differences between experimentally observed and theoretically calculated ν_{CH} are about 6, 4, 2, 2, 4, 6 and 2 cm^{-1}.

3.3. Thermodynamic parameters and molecular properties

Table 4 lists the calculated values of some thermodynamic parameters (such as zero-point vibrational energy, thermal corrections to energy, enthalpy and entropy) of the title compound. The minimum and maximum energy obtained from the geometric optimization of the title compound were calculated as -5224.102 a.u. for the B3LYP/6-311G(d,p) and -5210.664 a.u. for HF/6-31G(d,p) method. The calculated energy difference for these two extreme values is only -13.438 a.u. The biggest value of zero-point vibrational energy is 176.359 kcal/mol obtained at HF/6-31G(d,p) whereas the smallest one is 155.648 kcal/mol obtained at BLYP/6-311G(d,p). The total energies are found to decrease with the increase of basis set dimension [21].

The natural population analysis (NPA) and Mulliken charge values calculated for H_2L^{NNN} molecule are given in Tables 5 and 6, respectively. NPA and Mulliken atomic charge calculation results showed that the carbon atom in the carbonyl group (C19, 0.8379 (HF/6-31G(d, p)) have the highest positive charge. In addition, it was also found that the oxygen atom in the molecule (O2O, -0.7061 (HF/6-31G(d,p)) was charged with negative charge as expected and the C19-O20 carbonyl group shared the highest negative and positive charges of the molecule [21].

3.4. Hirshfeld surfaces analysis

The supramolecular architecture in the H_2L^{NNN} has been stabilized by hydrogen bonding, halogen···halogen and C-halogen···π (Cl···Cl and C-Cl···π) interactions. These interactions have further been investigated with the help of Hirshfeld surface analyses. Molecular Hirshfeld surface calculations were performed using the Crystal Explorer 17 program [40]. All Hirshfeld surfaces were created using crystallographically determined coordinates of the atoms in the compound and a standard (high) surface resolution [21,40]. The d_{norm}, d_e, d_i, curvedness and shape index surfaces of the H_2L^{NNN} are shown in Figure 3.

Table 3. Statistical comparison of theoretical and experimental vibrational wavenumbers of H_2L^{NNN} molecule on the used method and basis set *.

Method	**B3LYP**	**B3LYP×SF**	**B3LYP×CSF**	**B3LYP**	**B3LYP×SF**	**B3LYP×CSF**
Basis set	**6-31G(d,p)**			**6-311G(d,p)**		
r	0.9998	0.9998	0.9998	0.9998	0.9998	0.9998
Mean absolute percentage error	4.1492	0.4407	0.4648	3.7561	0.6706	0.6432
Mean absolute error	55.9474	5.8136	6.6174	49.3742	8.068	8.583
RMS	52.4182	12.5792	12.1672	46.3699	14.1371	13.2612
Scaling factor	1.000	0.9614	0.9588	1.000	0.9679	0.9639
Method	**B3PW91**	**B3PW91×SF**	**B3PW91×CSF**	**B3PW91**	**B3PW91×SF**	**B3PW91×CSF**
Basis set	**6-31G(d,p)**			**6-311G(d,p)**		
r	0.9998	0.9998	0.9998	0.9997	0.9997	0.9997
Mean absolute percentage error	4.8639	0.6422	0.6198	4.5332	0.8356	0.7321
Mean absolute error	63.8512	8.1063	8.5868	57.8698	9.4337	9.5315
RMS	58.0298	13.5511	13.1117	52.0289	14.3824	13.6441
Scaling factor	1.000	0.9573	0.9545	1.000	0.9631	0.9594
Method	**BLYP**	**BLYP×SF**	**BLYP×CSF**	**BLYP**	**BLYP×SF**	**BLYP×CSF**
Basis set	**6-31G(d,p)**			**6-311G(d,p)**		
r	0.9998	0.9998	0.9998	0.9998	0.9998	0.9998
Mean absolute percentage error	1.0796	1.2914	1.4114	1.1965	1.5784	1.3314
Mean absolute error	14.5717	14.9083	15.6016	14.694	17.0247	15.3341
RMS	19.0646	16.9564	16.7738	17.6689	17.9821	17.3735
Scaling factor	1.000	0.9945	0.9924	1.000	0.9934	0.9973
Method	**HF**	**HF×SF**	**HF×CSF**	**HF**	**HF×SF**	**HF×CSF**
Basis set	**6-31G(d,p)**			**6-311G(d,p)**		
r	0.9988	0.9988	0.9988	0.9987	0.9987	0.9987
Mean absolute percentage error	13.8217	3.1296	2.842	13.1963	3.2733	2.9543
Mean absolute error	171.1416	36.0217	34.4972	162.4022	37.3614	35.673
RMS	146.3035	34.4368	33.3818	138.9225	35.5478	34.3323
Scaling factor	1.000	0.8992	0.8928	1.000	0.9051	0.8981
Method	**mPW1PW**	**mPW1PW×SF**	**mPW1PW×CSF**	**mPW1PW**	**mPW1PW×SF**	**mPW1PW×CSF**
Basis set	**6-31G(d,p)**			**6-311G(d,p)**		
r	0.9997	0.9997	0.9997	0.9997	0.9997	0.9997
Mean absolute percentage error	5.8816	0.8467	0.7881	5.5286	1.1156	0.9195
Mean absolute error	75.9789	10.3949	10.5058	69.7615	12.1907	11.5181
RMS	67.5244	14.5200	14.1232	61.3765	15.8572	14.8462
Scaling factor	1.000	0.9500	0.9473	1.000	0.9567	0.9522

* SF: Scaling factor, CSF: Calculated Scaling factor in this research.

Table 4. The calculated thermodynamic parameters of H_2L^{NNN} molecule.

Thermodynamic parameters	**B3LYP**		**B3PW91**		**BLYP**		**HF**		**mPW1PW91**	
(298 K)	**6-31**	**6-311**	**6-31**	**6-311**	**6-31**	**6-311**	**6-31**	**6-311**	**6-31**	**6-311**
SCF energy (a.u.)	-5223.60	-5224.10	-5222.71	-5223.19	-5223.10	-5223.64	-5210.66	-5211.10	-5223.43	-5223.90
Total energy (Thermal) E_{total} (kcal/mol)	183.157	182.462	183.993	183.366	177.481	176.826	195.475	194.548	185.283	184.630
Entropy, S (cal/mol.K)	214.608	215.056	213.907	214.285	219.796	221.013	204.953	205.177	212.368	213.090
Vibrational energy, E_{vib} (kcal/mol)	181.379	180.685	182.216	181.588	175.704	175.048	193.697	192.770	183.506	182.852
Zero-point vib. energy, E_o (kcal/mol)	162.761	162.034	163.702	163.060	156.360	155.648	176.359	175.390	165.152	164.478
Rotational constant (GHz)										
A	0.09533	0.09686	0.09607	0.09805	0.09284	0.09397	0.09843	0.09881	0.09669	0.09864
B	0.08906	0.08832	0.08969	0.08941	0.08699	0.08610	0.08721	0.08757	0.09082	0.09047
C	0.06626	0.06592	0.06671	0.06660	0.06474	0.06428	0.06441	0.06481	0.06754	0.06733
Dipole moment (Debye)										
μ_x	-0.7187	-0.7558	-0.7122	-0.7230	-0.6796	-0.6568	-1.2741	-1.1995	-0.6052	-0.6577
μ_y	1.3092	1.4144	1.2573	1.2338	1.4447	1.6122	1.3005	1.3091	1.2777	1.2135
μ_z	4.2015	4.1790	4.2092	4.0901	4.3433	4.3486	3.2937	3.4107	4.2370	4.1058
μ_{Total}	4.4590	4.4761	4.4503	4.3329	4.6274	4.6841	3.7634	3.8452	4.4666	4.3316
Entropy (cal/mol.K)										
Total	214.608	215.056	213.907	214.285	219.796	221.013	204.953	205.177	212.368	213.090
Translational	45.208	45.208	45.208	45.208	45.208	45.208	45.208	45.208	45.208	45.208
Rotational	37.589	37.586	37.567	37.552	37.661	37.667	37.606	37.592	37.536	37.523
Vibrational	131.811	132.262	131.132	131.525	136.927	138.139	122.139	122.377	129.623	130.358

* 6-31: 6-31G(d,p); 6-311: 6-311G(d,p).

The 3D d_i surface was mapped using 0.956 (red) -2.976 (blue), d_e surface 0.957 (red) -2.977 (blue), and the d_{norm} surface -0.285 (red) -1.582 (blue) using fixed color scales (Figure 3) [21,46].

The d_{norm} is a ratio encompassing the distances of any surface point to the nearest interior (d_i) and exterior (d_e) atom and the van der Waals (vdW) radii of the atoms and calculated using Equation (2) [21,40,46-48].

$$d_{norm} = \frac{d_i - r_i^{vdW}}{r_i^{vdW}} + \frac{d_e - r_e^{vdW}}{r_e^{vdW}} \quad (2)$$

where, r_i^{vdW} and r_e^{vdW} are the vdW radii of the atoms. Feature d_{norm} is generally visualized as a color range from red ($d_{norm} < 0$), if the distance between interacting atoms is less than a sum of vdW radii, through white ($d_{norm} = 0$) to blue ($d_{norm} > 0$).

Table 5. The natural charges of the atoms of H_2L^{NNN} molecule determined by natural bond analysis (NBO) *.

Atom	Charge									
	B3LYP		B3PW91		BLYP		HF		mPW1PW91	
	6-31	6-311	6-31	6-311	6-31	6-311	6-31	6-311	6-31	6-311
C1	-0.2245	-0.1926	-0.2468	-0.2054	-0.2219	-0.2046	-0.2030	-0.1415	-0.2486	-0.2036
C2	0.6672	0.6546	0.6627	0.6480	0.6271	0.6202	0.8215	0.7960	0.6717	0.6557
O3	-0.5706	-0.5722	-0.5680	-0.5691	-0.5379	-0.5440	-0.6702	-0.6569	-0.5743	-0.5742
N4	-0.6418	-0.6342	-0.6434	-0.6354	-0.6113	-0.6070	-0.7401	-0.7185	-0.6501	-0.6418
C5	0.1720	0.1751	0.1700	0.1715	0.1627	0.1672	0.2031	0.2081	0.1725	0.1738
C6	-0.2417	-0.2047	-0.2506	-0.2104	-0.2382	-0.2033	-0.2279	-0.1872	-0.2525	-0.2122
C7	-0.2154	-0.1721	-0.2235	-0.1769	-0.2153	-0.1748	-0.2029	-0.1517	-0.2231	-0.1761
C8	-0.2396	-0.1991	-0.2482	-0.2042	-0.2349	-0.1969	-0.2341	-0.1882	-0.2499	-0.2055
C9	-0.2399	-0.2102	-0.2487	-0.2171	-0.2389	-0.2110	-0.2336	-0.1950	-0.2483	-0.2164
C10	0.0965	0.1147	0.0921	0.1115	0.0968	0.1152	0.1120	0.1266	0.0911	0.1106
N11	-0.4700	-0.5028	-0.4682	-0.4989	-0.4440	-0.4796	-0.5784	-0.6057	-0.4738	-0.5037
C12	0.1492	0.1630	0.1458	0.1587	0.1431	0.1574	0.1858	0.1965	0.1465	0.1591
C13	-0.2309	-0.1996	-0.2390	-0.2047	-0.2280	-0.1986	-0.2350	-0.1968	-0.2398	-0.2051
C14	-0.2221	-0.1775	-0.2303	-0.1828	-0.2206	-0.1791	-0.2024	-0.1525	-0.2311	-0.1833
C15	-0.2250	-0.1845	-0.2336	-0.1886	-0.2224	-0.1840	-0.2256	-0.1778	-0.2342	-0.1890
C16	-0.2349	-0.1937	-0.2430	-0.1995	-0.2323	-0.1942	-0.2150	-0.1713	-0.2443	-0.2004
C17	0.1427	0.1483	0.1395	0.1449	0.1390	0.1461	0.1500	0.1581	0.1402	0.1456
N18	-0.6204	-0.6051	-0.6228	-0.6034	-0.5931	-0.5809	-0.7326	-0.7030	-0.6270	-0.6069
C19	0.6806	0.6634	0.6745	0.6553	0.6399	0.6287	0.8379	0.8086	0.6836	0.6632
O20	-0.6094	-0.6165	-0.6050	-0.6120	-0.5745	-0.5860	-0.7061	-0.6988	-0.6127	-0.6185
C21	-0.2249	-0.1906	-0.2469	-0.2032	-0.2221	-0.2025	-0.2040	-0.1415	-0.2487	-0.2015
C22	0.6725	0.6651	0.6671	0.6580	0.6308	0.6280	0.8327	0.8144	0.6761	0.6660
O23	-0.5559	-0.5568	-0.5521	-0.5535	-0.5230	-0.5288	-0.6387	-0.6272	-0.5595	-0.5596
C24	-0.2190	-0.1901	-0.2404	-0.2023	-0.2162	-0.2011	-0.2029	-0.1474	-0.2418	-0.2005
Cl25	0.0686	0.0639	0.0754	0.0689	0.0680	0.0670	0.0561	0.0435	0.0764	0.0688
Cl26	0.0216	0.0193	0.0320	0.0255	0.0128	0.0163	0.0300	0.0153	0.0331	0.0253
Cl27	0.0475	0.0439	0.0555	0.0492	0.0433	0.0442	0.0399	0.0263	0.0570	0.0494
Cl28	0.0378	0.0369	0.0458	0.0424	0.0339	0.0365	0.0392	0.0258	0.0463	0.0418
Cl29	0.0884	0.0824	0.0953	0.0869	0.0911	0.0892	0.0704	0.0571	0.0956	0.0862
Cl30	0.0331	0.0260	0.0416	0.0324	0.0228	0.0204	0.0261	0.0116	0.0448	0.0342
Cl31	0.0581	0.0564	0.0672	0.0636	0.0532	0.0556	0.0499	0.0395	0.0686	0.0639
Cl32	0.0337	0.0330	0.0423	0.0389	0.0261	0.0299	0.0387	0.0269	0.0437	0.0390
Cl33	0.0588	0.0533	0.0664	0.0583	0.0568	0.0560	0.0475	0.0340	0.0679	0.0586
H34	0.4659	0.4476	0.4706	0.4522	0.4584	0.4423	0.4783	0.4465	0.4719	0.4535
H35	0.2772	0.2417	0.2858	0.2473	0.2742	0.2415	0.2641	0.2209	0.2868	0.2480
H36	0.2492	0.2085	0.2576	0.2131	0.2471	0.2092	0.2417	0.1935	0.2582	0.2132
H37	0.2490	0.2097	0.2574	0.2145	0.2469	0.2102	0.2418	0.1953	0.2580	0.2146
H38	0.2566	0.2203	0.2654	0.2269	0.2551	0.2215	0.2460	0.2020	0.2662	0.2271
H39	0.2607	0.2256	0.2698	0.2319	0.2583	0.2258	0.2540	0.2115	0.2705	0.2321
H40	0.2511	0.2109	0.2595	0.2157	0.2490	0.2115	0.2432	0.1952	0.2601	0.2158
H41	0.2510	0.2111	0.2592	0.2154	0.2490	0.2117	0.2427	0.1956	0.2598	0.2156
H42	0.2485	0.2121	0.2569	0.2169	0.2462	0.2125	0.2436	0.1984	0.2573	0.2167
H43	0.4480	0.4150	0.4546	0.4194	0.4425	0.4119	0.4557	0.4135	0.4555	0.4198

* 6-31: 6-31G(d,p); 6-311: 6-311G(d,p).

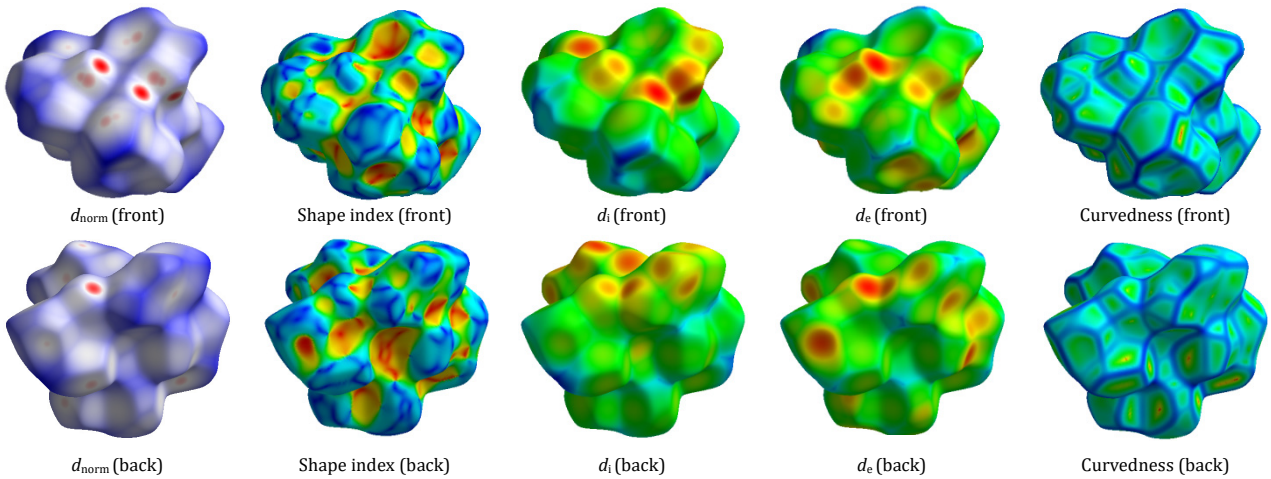

Figure 3. Hirshfeld surfaces mapped with d_{norm}, shape index, d_i, d_e and curvedness for H_2L^{NNN} molecule.

The fingerprint plot derived from the Hirshfeld surface is a 2D map that describes the type and quantitative amount of intermolecular interactions surrounding a molecule in a crystal lattice. The combination of the d_i and d_e functions in the form of a 2D fingerprint graph provides a summary of intermolecular contacts within the crystal.

The large red regions seen in the d_{norm} maps in Figure 4a represent strong H···O/O···H contacts. These contacts are attributed to N-H···O and C-H···O hydrogen bonds, which can also be seen in the 2D fingerprint plots as a pair of symmetrical spikes at $d_e + d_i \approx 2.2$ Å for the N-H···O interactions, and $d_e + d_i \approx 3.0$ Å for the C-H···O interactions.

Table 6. Mulliken charges of the atoms of H_2L^{NNN} molecule *.

Atom	Charge									
	B3LYP		B3PW91		BLYP		HF		mPW1PW91	
	6-31	6-311	6-31	6-311	6-31	6-311	6-31	6-311	6-31	6-311
C1	-0.3878	-0.4649	-0.4569	-0.5276	-0.3586	-0.4528	-0.4048	-0.3923	-0.4685	-0.5326
C2	0.6395	0.4897	0.6527	0.5171	0.5966	0.4449	0.8018	0.6579	0.6643	0.5276
O3	-0.4480	-0.3114	-0.4492	-0.3201	-0.4179	-0.2762	-0.5397	-0.4266	-0.4555	-0.3259
N4	-0.6368	-0.4570	-0.6594	-0.4837	-0.5809	-0.4136	-0.8184	-0.6047	-0.6727	-0.4916
C5	0.3349	0.2574	0.3430	0.2798	0.3265	0.2417	0.3310	0.2916	0.3461	0.2855
C6	-0.0958	-0.0623	-0.1247	-0.0681	-0.0797	-0.0601	-0.1208	-0.0514	-0.1269	-0.0650
C7	-0.0916	-0.0856	-0.1294	-0.0960	-0.0651	-0.0798	-0.1475	-0.0758	-0.1347	-0.0933
C8	-0.0917	-0.0803	-0.1280	-0.0867	-0.0640	-0.0736	-0.1551	-0.0818	-0.1337	-0.0846
C9	-0.0913	-0.0398	-0.1187	-0.0470	-0.0734	-0.0315	-0.1456	-0.0581	-0.1199	-0.0435
C10	0.1374	-0.0607	0.1086	-0.0980	0.1469	-0.0538	0.1656	0.0294	0.1018	-0.1065
N11	-0.6031	-0.4362	-0.6079	-0.4453	-0.5511	-0.3910	-0.8135	-0.6306	-0.6215	-0.4547
C12	0.2820	0.1549	0.2767	0.1522	0.2736	0.1389	0.3004	0.2287	0.2785	0.1559
C13	-0.1044	-0.0532	-0.1314	-0.0576	-0.0855	-0.0482	-0.1515	-0.0659	-0.1346	-0.0561
C14	-0.0894	-0.0812	-0.1267	-0.0921	-0.0629	-0.0741	-0.1407	-0.0733	-0.1321	-0.0908
C15	-0.0813	-0.0755	-0.1187	-0.0837	-0.0533	-0.0695	-0.1505	-0.0793	-0.1243	-0.0806
C16	-0.1202	-0.0721	-0.1528	-0.0834	-0.1000	-0.0674	-0.1323	-0.0532	-0.1571	-0.0840
C17	0.3058	0.1960	0.3032	0.2094	0.3016	0.1868	0.2713	0.2278	0.3056	0.2151
N18	-0.5842	-0.4239	-0.6079	-0.4457	-0.5307	-0.3809	-0.7828	-0.5914	-0.6177	-0.4515
C19	0.6528	0.5055	0.6604	0.5188	0.6082	0.4654	0.8222	0.6678	0.6726	0.5270
O20	-0.4740	-0.3510	-0.4708	-0.3534	-0.4393	-0.3129	-0.5695	-0.4648	-0.4801	-0.3608
C21	-0.3906	-0.4546	-0.4598	-0.5136	-0.3614	-0.4462	-0.3998	-0.3641	-0.4721	-0.5194
C22	0.6178	0.4376	0.6231	0.4474	0.5754	0.4029	0.7876	0.5924	0.6349	0.4553
O23	-0.4403	-0.2864	-0.4342	-0.2878	-0.4142	-0.2566	-0.5087	-0.3851	-0.4404	-0.2931
C24	-0.3670	-0.4258	-0.4326	-0.4810	-0.3401	-0.4190	-0.3827	-0.3427	-0.4441	-0.4856
Cl25	0.0836	0.0863	0.1038	0.1024	0.0738	0.0836	0.0910	0.0609	0.1080	0.1035
Cl26	0.0338	0.0418	0.0568	0.0610	0.0183	0.0323	0.0575	0.0348	0.0603	0.0629
Cl27	0.0632	0.0707	0.0839	0.0882	0.0514	0.0646	0.0711	0.0462	0.0881	0.0901
Cl28	0.0566	0.0719	0.0771	0.0896	0.0453	0.0649	0.0702	0.0526	0.0805	0.0913
Cl29	0.1078	0.1127	0.1281	0.1282	0.1008	0.1130	0.1076	0.0823	0.1318	0.1288
Cl30	0.0577	0.0573	0.0773	0.0742	0.0414	0.0472	0.0607	0.0270	0.0832	0.0787
Cl31	0.0781	0.0834	0.1016	0.1040	0.0638	0.0753	0.0914	0.0582	0.1059	0.1062
Cl32	0.0481	0.0646	0.0683	0.0829	0.0339	0.0545	0.0676	0.0522	0.0723	0.0853
Cl33	0.0732	0.0809	0.0934	0.0975	0.0630	0.0774	0.0771	0.0562	0.0979	0.0994
H34	0.3393	0.3156	0.3523	0.3194	0.3125	0.2996	0.4081	0.3440	0.3578	0.3211
H35	0.1415	0.1388	0.1785	0.1524	0.1124	0.1283	0.2021	0.1350	0.1843	0.1506
H36	0.1019	0.1061	0.1378	0.1154	0.0748	0.0978	0.1677	0.1095	0.1435	0.1138
H37	0.0995	0.1035	0.1357	0.1125	0.0724	0.0953	0.1664	0.1072	0.1413	0.1106
H38	0.1145	0.1276	0.1505	0.1436	0.0882	0.1179	0.1837	0.1284	0.1559	0.1424
H39	0.1187	0.1309	0.1563	0.1476	0.0909	0.1210	0.1904	0.1346	0.1620	0.1469
H40	0.1051	0.1076	0.1410	0.1163	0.0779	0.0994	0.1710	0.1109	0.1466	0.1144
H41	0.1042	0.1067	0.1400	0.1154	0.0771	0.0986	0.1688	0.1092	0.1456	0.1135
H42	0.1056	0.1111	0.1424	0.1217	0.0783	0.1038	0.1746	0.1098	0.1478	0.1197
H43	0.2946	0.2632	0.3164	0.2736	0.2733	0.2522	0.3565	0.2866	0.3192	0.2740

* 6-31: 6-31G(d,p); 6-311: 6-311G(d,p).

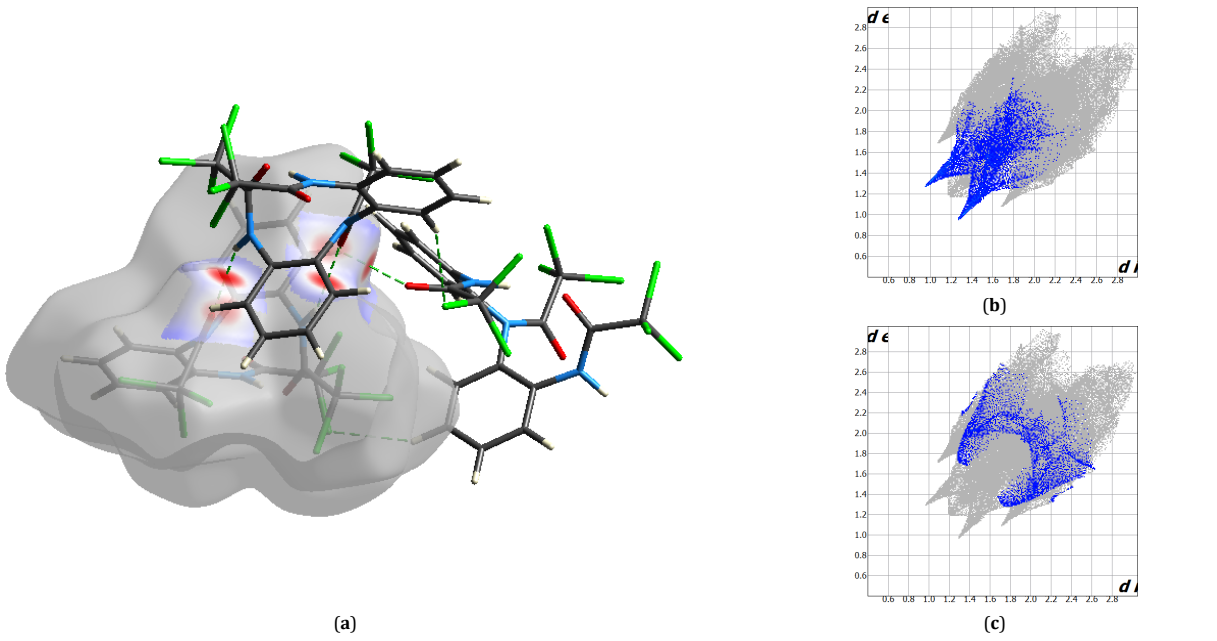

Figure 4. (a) A view of d_{norm} Hirshfeld surface for close N–H···O and C-H···O contacts (b) Decomposed fingerprint plot for N–H···O contacts. (c) Decomposed fingerprint plot for C–H···O contacts.

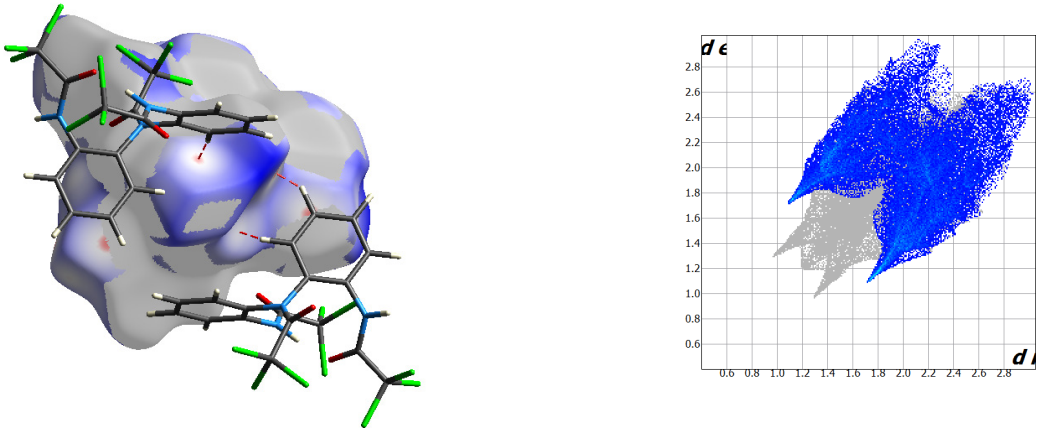

(**a**) (**b**)

Figure 5. (a) A view of d_{norm} Hirshfeld surface for close Cl···H contacts (b) Decomposed fingerprint plot for Cl···H contacts.

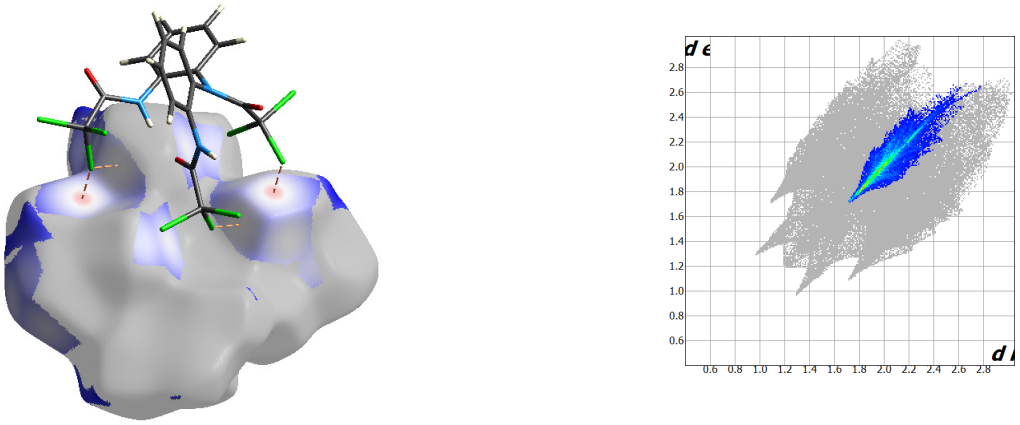

(**a**) (**b**)

Figure 6. (a) A view of d_{norm} Hirshfeld surface for close Cl···Cl contacts (b) Decomposed fingerprint plot for Cl···Cl contacts.

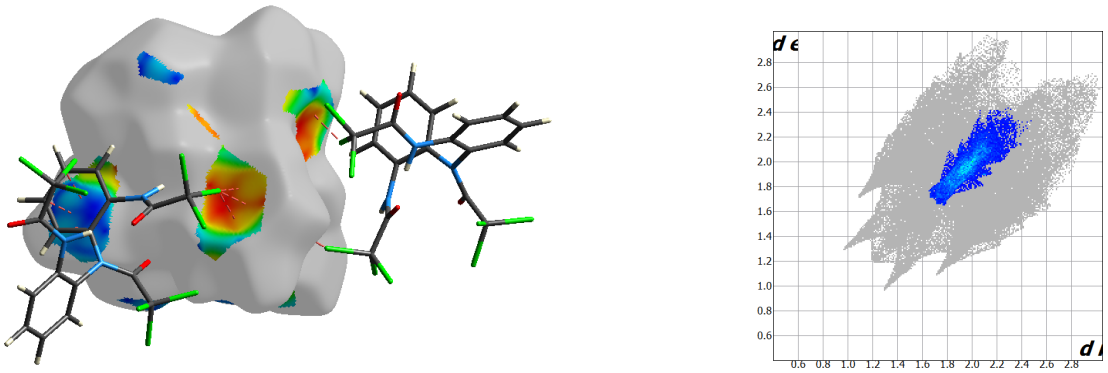

(**a**) (**b**)

Figure 7. (a) A view of d_{norm} Hirshfeld surface for close C-Cl···π contacts (b) Decomposed fingerprint plot for C-Cl···π contacts.

The H···O/O···H contacts are important for a compound with 7.3% contribution to the Hirshfeld surface area (see Figure 4b and c).

The largest portion of the total Hirshfeld surface belongs to Cl···H/H···Cl contacts with 43.3%. These interactions are represented as a pair of short spikes at $d_e + d_i \approx 2.8$ Å in fingerprint plot and seen as slight red spots on the d_{norm} Hirshfeld Surface (Figure 5).

Other important interactions that occur on the Hirshfeld surface mapped with the d_{norm} function of the compound H_2L^{NNN} are the Cl-Cl interaction, which contribute 18.8% to the Hirshfeld surface. In the decomposed 2D fingerprint plot, the shortest contact between Cl atoms is also shorter than the sum of vdW radii with $d_e + d_i \approx 3.4$ Å. Therefore, these interactions are essential intermolecular contacts in the crystal self-assembly of the molecule (Figure 6).

The C-Cl···π interactions, which happened between the Cl atom and the π-system of adjacent phenyl, contributing to the three-dimensional structure of the synthesized H_2L^{NNN} compound were visualized by means of the Hirshfeld surface

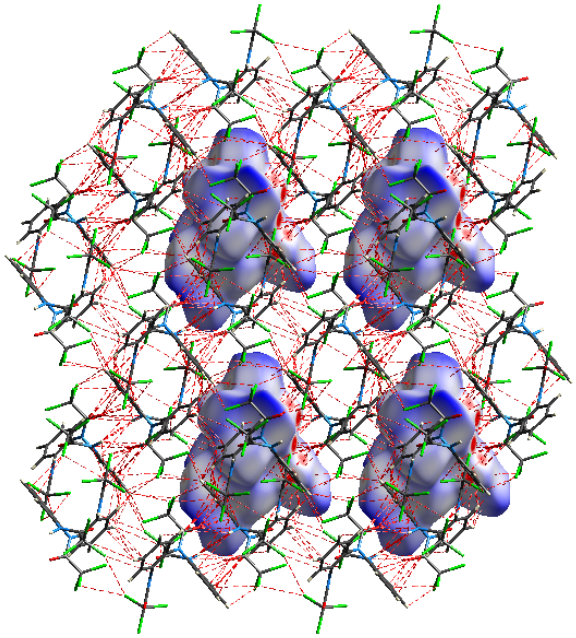

Figure 8. All contacts in the crystal lattice of the compound H_2L^{NNN}.

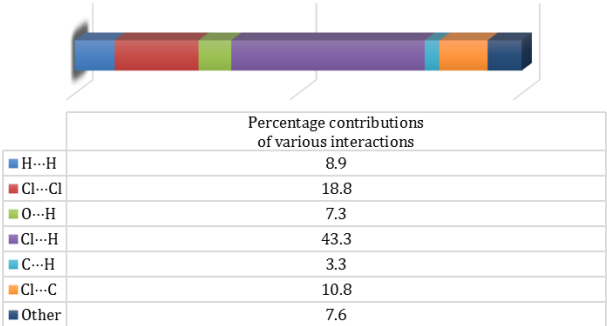

Figure 9. Relative percentage contributions to the Hirshfeld surface area of various intermolecular contacts in H_2L^{NNN}.

mapped by the shape index function. As can be seen from Figure 7, on the Hirshfeld surface mapped by the shape index function, the hollow orange areas correspond to the C-$Cl_{external}\cdots\pi_{internal}$ and the bumps blue areas correspond to the C-$Cl_{internal}\cdots\pi_{external}$ interactions. These interactions contribute 10.8% to total Hirshfeld surface and the separated 2D fingerprint plot of C-Cl···π interactions show that the shortest contact is $d_e + d_i \approx 3.4$ Å (Figure 7b).

On the other hand, H···H contacts, *i.e.* dispersion interactions, contribute 8.9% of the total number of contacts of the compound. However, the shortest H···H contact is $d_e + d_i \approx$ 2.4 Å, which is longer than the vdW radii totals. Therefore, the compound in the crystal package is not from the main intermolecular contacts. All contacts in the crystal lattice of the compound H_2L^{NNN} and the proportions of these contacts are shown in Figures 8 and 9, respectively.

4. Conclusion

The ground state geometries for the H_2L^{NNN} were optimized using the HF, BLYP, B3LYP, B3PW91 and mPW1PW91 functionals with 6-31G(d,p) and 6-311G(d,p) basis sets. The harmonic vibrational frequencies were also calculated and scaled values have been compared with an experimental IR spectrum. The correlation between the calculated and experimental vibration frequencies is characterized by coefficients bigger than 0.9987 for all used methods. Any discrepancy noted between the observed and the calculated frequencies may be due to the fact that the calculations have been actually done on a single molecule in the gaseous state contrary to the experimental values recorded in the presence of intermolecular interactions. The computed IR spectrum of the H_2L^{NNN} molecule is in good agreement with its observed FT-IR spectrum. The IR spectrum of the H_2L^{NNN} compound was interpreted in terms of the potential energy distribution analysis. Optimal uniform scaling factors were also calculated. On the other hand, the supramolecular architecture of H_2L^{NNN} was investigated by the X-rays single crystal analysis and Hirshfeld surface analysis. It was found that the supramolecular structure in H_2L^{NNN} was stabilized by hydrogen bonding, halogen···halogen and C-halogen···π (Cl···Cl and C-Cl···π) interactions.

Acknowledgements

This study was supported by Research Fund of Mersin University in Turkey with Project Number: 2018-1-TP2-2799.

Supporting information

CCDC-1951022 contains the supplementary crystallographic data for this paper. These data can be obtained free of charge via https://www.ccdc.cam.ac.uk/structures/, or by e-mailing data_request@ccdc.cam.ac.uk, or by contacting The Cambridge Crystallographic Data Centre, 12 Union Road, Cambridge CB2 1EZ, UK; fax: +44(0)1223-336033.

Disclosure statement

Conflict of interests: The authors declare that they have no conflict of interest.
Author contributions: All authors contributed equally to this work.
Ethical approval: All ethical guidelines have been adhered.
Sample availability: Samples of the compounds are available from the author.

Funding

Mersin University
http://dx.doi.org/10.13039/501100004172

ORCID

İmmihan Sezen Aydogdu
http://orcid.org/0000-0002-7334-0562
Ilkay Gumus
http://orcid.org/0000-0002-9398-0057
Hakan Arslan
http://orcid.org/0000-0003-0046-9442

References

[1]. Lyaskovskyy, V.; Bruin, B. *ACS Catal.* **2012**, *2*, 270-279.
[2]. Meunier, B.; Visser, S. P.; Shaik, S. *Chem. Rev.* **2004**, *104(9)*, 3947-3980.
[3]. Allgeier, A. M.; Mirkin, C. A. *Angew. Chem. Int. Ed.* **1998**, *37*, 894-908.
[4]. Kuchynka, D. J.; Kochi, J. K. *Inorg. Chem.* **1988**, *27*, 2574-2581.
[5]. Bart, S. C.; Lobkovsky, E.; Bill, E.; Chirik, P. J. *J. Am. Chem. Soc.* **2006**, *128(16)*, 5302-5303.
[6]. Tondreau, A. M.; Milsmann, C.; Patrick, A. D.; Hoyt, H. M.; Lobkovsky, E.; Wieghardt, K.; Chirik, P. J. *J. Am. Chem. Soc.* **2010**, *132(42)*, 15046-15059.
[7]. Bowman, A. C.; Milsmann, C.; Hojilla, A. C. C.; Lobkovsky, E.; Wieghardt, K.; Chirik, P. J. *J. Am. Chem. Soc.* **2010**, *132(5)*, 1676-1684.
[8]. Bowman, C. A.; Milsmann, C.; Bill, E.; Lobkovsky, E.; Weyhermüller, T.; Wieghardt , K.; Chirik, P. J. *Inorg. Chem.* **2010**, *49(13)*, 6110-6123.
[9]. Manuel, T. D.; Rohde, J. U. *Am. Chem. Soc.* **2009**, *131(43)*, 15582-15583.
[10]. Pierpont, C. G.; Lange, C. W. *Prog. Inorg. Chem.* **2007**, *41(1)*, 331-442.
[11]. Pierpont, C. G.; Buchanan, R. M. *Coord. Chem. Rev.* **1981**, *38(1)*, 45-87.
[12]. Pierpont, C. G. *Coord. Chem. Rev.* **2001**, *219-221*, 415-433.
[13]. Rolle, C. J.; Hardcastle, K. I.; Soper, J. D. *Inorg. Chem.* **2008**, *47(6)*, 1892-1894.
[14]. Mukherjee, C.; Pieper, U.; Bothe, E.; Bachler, V.; Bill, E.; Weyhermuller, T.; Chaudhuri, P. *Inorg. Chem.* **2008**, *47(19)*, 8943-8956.
[15]. Bill, E.; Bothe, E.; Chaudhuri, P.; Chlopek, K.; Herebian, D.; Kokatam, S. *Chem. Eur. J.* **2005**, *11(1)*, 204-224.
[16]. Chun, H.; Verani, C. N.; Chaudhuri, P.; Bothe, E.; Bill, E.; Weyhermuller, T.; Wieghardt, K. *Inorg. Chem.* **2001**, *40(17)*, 4157-4166.
[17]. Wile, B. M.; Trovitch, R. J.; Bart, S. C.; Tondreau, A. M.; Lobkovsky, E.; Milsmann, C.; Bill, E.; Wieghardt, K.; Chirik, P. J. *Inorg. Chem.* **2009**, *48(9)*, 4190-4200.
[18]. Vlcek, A. *Coord. Chem. Rev.* **2010**, *254(13-14)*, 1357-1357.
[19]. Skabara, P. J.; Pozo-Gonzalo, C.; Lardies, M. N.; Laguna, M.; Cerrada, E.; Luquin, A.; Gonzalez, B.; Coles, S. J.; Hursthouse, M. B.; Harrington, R. W.; Clegg, W. *Dalton Trans.* **2008**, *23*, 3070-3079.
[20]. Ward, M. D.; McCleverty, J. A. *J. Chem. Soc. Dalton Trans.* **2002**, *3*, 275-288.
[21]. Aydogdu, S. I., MSc Thesis, Mersin University, Mersin, Turkey, 2019.
[22]. Aydogdu, I.; Gumus, I.; Arslan, H. Int. Eng. Nat. Sci. Conf. Book, Diyarbakir, Turkey, 2019
[23]. Polat, A. S., MSc Thesis, Mersin University, Mersin, Turkey, 2019.
[24]. Arslan, H. Ligand design studies for metal catalyzed oxidation reactions, TUBITAK Project no: 112T322 (2012).
[25]. Frisch, M. J.; Trucks, G. W.; Schlegel, H. B.; Scuseria, G. E.; Robb, M. A.; Cheeseman, J. R.; Scalmani, G.; Barone, V.; Petersson, G. A.; Nakatsuji, H.; Li, X.; Caricato, M.; Marenich, A. V.; Bloino, J.; Janesko, B. G.; Gomperts, R.; Mennucci, B.; Hratchian, H. P.; Ortiz, J. V.; Izmaylov, A. F.; Sonnenberg, J. L.; Williams-Young, D.; Ding, F.; Lipparini, F.; Egidi, F.; Goings, J.; Peng, B.; Petrone, A.; Henderson, T.; Ranasinghe, D.; Zakrzewski, V. G.; Gao, J.; Rega, N.; Zheng, G.; Liang, W.; Hada, M.; Ehara, M.; Toyota, K.; Fukuda, R.; Hasegawa, J.; Ishida, M.; Nakajima, T.; Honda, Y.; Kitao, O.; Nakai, H.; Vreven, T.; Throssell, K.; Montgomery, J. A.; Jr.; Peralta, J. E.; Ogliaro, F.; Bearpark, M. J.; Heyd, J. J.; Brothers, E. N.; Kudin, K. N.; Staroverov, V. N.; Keith, T. A.; Kobayashi, R.; Normand, J.; Raghavachari, K.; Rendell, A. P.; Burant, J. C.; Iyengar, S. S.; Tomasi, J.; Cossi, M.; Millam, J. M.; Klene, M.; Adamo, C.; Cammi, R.; Ochterski, J. W.; Martin, R. L.; Morokuma, K.; Farkas, O.; Foresman, J. B.; Fox, D. J. Gaussian 16, Revision C.01, Gaussian, Inc.; Wallingford CT, 2016.
[26]. Foresman, B.; Frisch, E. Exploring Chemistry with Electronic Structure Methods: a Guide to Using Gaussian, Gaussian Pitttsburg, PA, 1993.
[27]. Scott, A. P.; Radom, L. *J. Chem.* **1996**, *100*, 16502-16513.
[28]. Arslan, H.; Algul, O.; Dundar, Y. *Vib. Spectrosc.* **2007**, *44*, 248-255
[29]. Arslan, H.; Algul, O. *Spectrochim. Acta A* **2008**, *70*, 109-116
[30]. Yabalak, E.; Gunay, F.; Kasumov, V.; Arslan, H. *Spectrochim. Acta A* **2013**, *110*, 291-303
[31]. Arslan, H.; Mansuroglu, D.; Vanderveer, D.; Binzet, G. *Spectrochim. Acta A* **2009**, *72*, 561-571.
[32]. Arslan, H.; Demircan, A. *Int. J. Mol. Sci.* **2007**, *8*, 1064-1082.
[33]. Arslan, H.; Floerke, U.; Kulcu, N.; Binzet, G. *Spectrochim. Acta A* **2007**, *68*, 1347-1355.
[34]. Dennington, R. Keith, T. A.; Millam, J. M. GaussView, Version 6, Semichem Inc.; Shawnee Mission, KS, 2016.
[35]. Panchenko, Y. N. *J. Mol. Struct.* **2001**, *567-568*, 217-230.
[36]. Rauhut, G.; Pulay, P. *J. Phys. Chem.* **1995**, *99(10)*, 3093-3100.
[37]. Arslan, H., Performance Analysis of Vibrational Frequencies, 1.0, Mersin, Turkey, 2007.
[38]. Reed, A. E.; Curtiss, L. A.; Weinhold, F. *Chem. Rev.* **1988**, *88(6)*, 899-926.
[39]. Glendening, E. D.; Reed, A. E.; Carpenter, J. E.; Weinhold, F. J. *Am. Chem. Soc.* **1998**, *120(46)*, 12051-12068.
[40]. Turner, M. J.; McKinnon, J. J.; Wolff, S. K.; Grimwood, D. J.; Spackman, P. R.; Jayatilaka, D.; Spackman, M. A. CrystalExplorer17, University of Western Australia, http://hirshfeldsurface.net, 2017
[41]. Krishnakumar, V.; Dheivamalar, S.; Xavier, R. J.; Balachandran, V. *Spectrochim. Acta A* **2006**, *65(1)*, 147-154.
[42]. Arslan, H.; Florke, U.; Kulcu, N. *Spectrochim. Acta A* **2007**, *67(3-4)*, 936-943.
[43]. Yesilkaynak, T.; Binzet, G.; Emen, F. M.; Florke, U.; Kulcu, N.; Arslan, H. *Eur. J. Chem.* **2010**, *1(1)*, 1-5.
[44]. Arslan, B., MSc Thesis, Mersin University, Mersin, Turkey, 2017.
[45]. Aslantatar, E., MSc Thesis, Mersin University, Mersin, Turkey, 2013.
[46]. Spackman, M.; Jayatilaka, D. *CrystEngComm.* **2009**, *11*, 19-32.
[47]. McKinnon, J. J.; Jayatilaka, D.; Spackman, M. A. *Chem. Commun.* **2007**, *267*, 3814-3816;
[48]. McKinnon, J. J.; Mitchell, A. S.; Spackman, M. A. *Chem. A Eur. J.* **1998**, *4*, 2136-214.

Copyright © 2019 by Authors. This work is published and licensed by Atlanta Publishing House LLC, Atlanta, GA, USA. The full terms of this license are available at http://www.eurjchem.com/index.php/eurjchem/pages/view/terms and incorporate the Creative Commons Attribution-Non Commercial (CC BY NC) (International, v4.0) License (http://creativecommons.org/licenses/by-nc/4.0). By accessing the work, you hereby accept the Terms. This is an open access article distributed under the terms and conditions of the CC BY NC License, which permits unrestricted non-commercial use, distribution, and reproduction in any medium, provided the original work is properly cited without any further permission from Atlanta Publishing House LLC (European Journal of Chemistry). No use, distribution or reproduction is permitted which does not comply with these terms. Permissions for commercial use of this work beyond the scope of the License (http://www.eurjchem.com/index.php/eurjchem/pages/view/terms) are administered by Atlanta Publishing House LLC (European Journal of Chemistry).